Chemical Engineering Journal Advances 21 (2025) 100707

Contents lists available at ScienceDirect

Chemical Engineering Journal Advances

journal homepage: www.sciencedirect.com/journal/chemical-engineering-journal-advances

Occurrence of micropollutants in surface water and removal by catalytic wet peroxide oxidation enhanced filtration using polymeric membranes loaded with carbon nanotubes

Adriano S. Silva [a,b,c,d,*], Paulo Zadra Filho [a,e], Ana Paula Ferreira [a,f], Fernanda F. Roman [a,c,d], Arthur P. Baldo [a], Madeleine Rauhauser [g], Jose L. Diaz de Tuesta [h], Ana I. Pereira [b], Adrián M.T. Silva [c,d], Juliana M.T. Pietrobelli [e], Marzhan S. Kalmakhanova [i], Daniel D. Snow [g], Helder T. Gomes [a,*]

[a] CIMO, LA SusTEC, Instituto Politécnico de Bragança, Campus de Santa Apolónia, 5300-253 Bragança, Portugal
[b] CeDRI, SusTEC, Instituto Politécnico de Bragança, Campus de Santa Apolónia, 5300-253, Bragança, Portugal
[c] LSRE-LCM - Laboratory of Separation and Reaction Engineering – Laboratory of Catalysis and Materials, Faculty of Engineering, University of Porto, Rua Dr. Roberto Frias, 4200-465 Porto, Portugal
[d] ALiCE - Associate Laboratory in Chemical Engineering, Faculty of Engineering, University of Porto, Rua Dr. Roberto Frias, 4200-465 Porto, Portugal
[e] Academic Department of Chemical Engineering. Universidade Tecnológica Federal do Paraná—UTFPR, Ponta Grossa 84017-220, PR, Brazil
[f] Chemistry Center of Vila Real (CQVR), University of Trás-os-Montes and Alto Douro, Quinta de Prados, 5000-801 Vila Real, Portugal
[g] Water Sciences Laboratory, Nebraska Water Center, Part of Daugherty Water for Food Global Institute, and School of Natural Resources, University of Nebraska, Lincoln, NE 68583-0844, USA
[h] Chemical and Environmental Engineering Group, ESCET, Universidad Rey Juan Carlos, c/Tulipán s/n, 28933 Móstoles, Spain
[i] Department of Chemistry and Chemical Technology, M. Kh. Dulaty Taraz University, 080012 Taraz, Kazakhstan

ARTICLE INFO

Keywords:
POCIS
CECs
WWTPs efficiency
CNTs
Membrane technology

ABSTRACT

Monitoring campaigns of contaminants of emerging concern (CECs) in surface waters is of utmost importance in evaluating the anthropogenic impact on riparian ecosystems. Beyond identifying pollutants and threats, treatment solutions are also needed to mitigate the adverse effects caused by polluted water discharged into the environment. For years, grab samples have been used to assess water quality, but the results can be misleading since contaminants are not always found due to the low and highly variable concentrations at which they are present in these matrices. Even in such small concentrations, the contaminants can be harmful to aquatic life. Therefore, for about three months, passive samplers were used to monitor the presence of pharmaceuticals in river water up- and downstream the discharge of a wastewater treatment plant (WWTP). Passive samplers were extracted, analyzed and the results were used to identify possible pollution composition and potential sources. Our campaign enabled the identification and quantification of 28 contaminants and showed that 27 increased in amount after WWTP discharge entered the river. The statistical analysis revealed the correlation between the pollutants, showed the oscillation in their amounts, and enabled the identification of specific pollutant groups that deserve attention for treatment, such as antibiotics and antidepressants. Moreover, an innovative catalytic wet peroxide oxidation (CWPO) intensified filtration process was investigated as a possible water treatment solution, using composite polymeric membranes loaded with carbon nanotubes (CNTs). Sulfamethoxazole (SMX) was selected as a model pollutant, and 85–90 % removals were achieved in continuous flow mode during 8 h (equivalent to 2255–2315 mg m^{-2} h^{-1}).

1. Introduction

Water scarcity is one of the main concerns in the 21st century [1]. The increasing global population and industrialization significantly affect the availability of clean water. The problem will persist and increase in dimension as the population and economies continue to grow

* Corresponding authors.
E-mail addresses: adriano.santossilva@ipb.pt (A.S. Silva), htgomes@ipb.pt (H.T. Gomes).

https://doi.org/10.1016/j.ceja.2025.100707

Available online 10 January 2025

[2]. The United Nations (UN) estimates that 1.8 billion people will live in water scarcity in 2025, and two-thirds of the population will live under water-stressed conditions [3]. The current solution to fight water scarcity is the diversification of water sources. Despite the possibility of purifying water via novel technologies, such as desalination [4] and fog water harvesting [5], these solutions are often expensive and highly dependent on the geographical conditions of the region. Therefore, wastewater treated by innovative processes is another complementary solution to tackle water scarcity [6].

The design of efficient wastewater treatment plants (WWTPs) is a task that demands a lot of effort, considering the complexity of the waste stream arriving at these sites [7]. Monitoring the concentration of pollutants in water bodies is also essential to investigate the efficiency of WWTPs and help the authorities in the identification of possible needs to improve the operations [8]. Most conventional monitoring campaigns employ the grab sampling method to collect water samples to analyze the concentration of chemical compounds. However, this method can lead to erroneous conclusions since the variation of the pollutant concentration over time may prevent detection by means of spot sampling [9]. This limitation can be overcome by using passive samplers deployed at a designed location. There are several options for passive samplers, but the polar organic chemical integrative sampler (POCIS) represents a suitable option to monitor contamination by compounds with log K_{OW} (octanol/water) coefficient ranging from 0 to 4 [10]. Many contaminants can be monitored with POCIS, such as pharmaceutical substances, pesticides and personal care products.

Many studies reported pollutant monitoring campaigns using POCIS. For instance, Mathon et al. have demonstrated the value of using POCIS to improve the data quality on contaminants monitoring, decreasing in the Limit of Quantification (LoQ) for almost all contaminants (by a factor of 3 to 84) [11]. Severson et al. used POCIS throughout the United States for illegal drug monitoring and detection, showing a feasible way to implement the technology in a wide variety of communities [12]. Brunelle et al. used POCIS to study the behavior of contaminants of emerging concern (CECs) in *De facto* water reuse. This occurs when a wastewater treatment facility discharges treated water into a surface water body located upstream of a drinking water treatment plant's intake. Their study identified over 100 CECs in watersheds and 28 CECs in treated drinking water [13]. In another work, Metcalfe et al. demonstrated the importance of using passive samplers for monitoring campaigns by comparing grab samples results with passive samplers [14]. In their case, the contaminants in grab samples from drinking water were below detection limits, whereas POCIS samplers allowed the detection and quantification of several contaminants. This result allowed the assessment of the differences in removal efficiencies between and within treatment plants. Several other research papers discuss monitoring contaminants with POCIS, reinforcing the need to search for suitable alternatives to treat the polluted streams [15–17].

Among the technologies employed for wastewater treatment, advanced oxidation processes (AOPs) deserve special attention [18–21]. These technologies are based on the generation of reactive oxygen species such as the hydroxyl ($HO^{\bullet}$, $E^{\circ} = 2.5 - 3.1\ V_{NHE}$ [22]), superoxide ($O_2^{\bullet-}$, $E^{\circ} = 0.33\ V_{NHE}$ [23]), and persulfate radicals ($SO_4^{\bullet-}$, $E^{\circ} = 2.7\ V_{NHE}$ [22]). Several papers reported the application of these technologies to degrade a wide range of pollutants, such as sulfamethoxazole (SMX), an antibiotic whose presence in river water can cause severe harmful effects. For instance, Li et al. reported the use of Co and Fe supported in zeolite (ZSM-5) to degrade 93 % of SMX in 60 min using peroxymonosulfate as oxidant [24]. Another study, published by Ma et al., reported the application of ozonation to completely degrade SMX in 15 min of reaction using ZSM-5 zeolite to reduce the consumption of ozone in the process [25]. Photocatalysis was also employed to degrade SMX, as shown by Dang et al. in their study, reaching 89 % degradation in 4 h of reaction using TiO_2 doped with biochar as photocatalyst [26]. The degradation of SMX by heterogeneous Fenton was also reported in the literature, with the results obtained by Ribeiro et al. using magnetic carbon xerogels as a catalyst showing complete removal of the pollutant within 30 min of reaction at optimized operating conditions [27]. Despite the interesting advances previously reported, the experiments are mostly limited to batch essays.

The challenges for large-scale implementation of most AOPs are related to the associated costs since many require specific installations with complex specifications to operate [28]. Among these technologies, catalytic wet peroxide oxidation (or heterogeneous Fenton, when using iron-based catalysts) has shown promising results for removing persistent organic pollutants. Different catalysts have already been explored for this application, from metal-based to carbon-based ones. In a previous work, it was demonstrated that CNTs synthesized from plastic solid wastes have applicability as catalysts in the CWPO process [29]. However, alternatives should be studied to explore CNTs immobilization solutions to facilitate recovery and possible process scale-up.

In this study, an extended monitoring campaign was performed in the northeast region of Portugal, using POCIS for a period of 3 months (June, July and August 2023). The campaign was planned to monitor the quality of the river water, upstream and downstream the local WWTP. The results obtained from the campaign pointed out the inefficient removal of CECs in the WWTP. Antibiotics, such as sulfamethoxazole (SMX), were found in concerning amounts in the river water. SMX was chosen as model pollutant to assess the efficiency of the proposed CWPO-intensified filtration solution, based on PVP/PVDF CNT-composite polymeric membranes for the degradation of organic pollutants.

2. Methodology

2.1. Reagents

The reagents used for the monitoring campaign are described in Table S1. The precursors used in the preparation of the CNTs, namely low-density polyethylene (LDPE, with an average molecular weight ~35,000 g mol^{-1}, and average molecular number ~7700) were supplied by Sigma-Aldrich. The catalyst used in chemical vapor deposition (CVD) to synthesize CNTs was prepared using iron (II) chloride tetrahydrate (98 %), iron (III) chloride hexahydrate (97 %), absolute ethanol (99.8 %), and ethylene glycol (99 %), obtained from Acros Organics, VWR Chemicals, Fisher Chemical, and Fisher Chemical, respectively. Alumina was supplied by BASF in pellet form. Prior to use, it was ground and sieved (53–106 μm). Sulfuric acid (95 %) from VWR Chemicals was used to purify CNTs. Polyvinylpyrrolidone (PVP; MW: 40,000 g mol^{-1}), 1-methyl-2-pyrrolidone (NMP; 99.5 wt.%) and poly(vinylidene fluoride) (PVDF; average molecular weight: 275,000 g mol^{-1}) were supplied by Sigma Aldrich and used for polymeric membrane fabrication.

In CWPO-intensified filtration experiments, SMX (98 wt.%) and hydrogen peroxide (H_2O_2, 30 w/*v*%), supplied by Alfa Aesar and VWR Chemicals, respectively, were used. For analytical measurements, orthophosphoric acid (85 w/*v*%), sodium sulphite anhydrous (98 wt.%), titanium (IV) oxysulfate (99.99 wt.% metal basis, *c.a.* 15 wt.% solution in dilute sulfuric acid) were obtained from Sigma Aldrich. All chemicals were used as received. Ultrapure and distilled water were used to prepare solutions and washing procedures, respectively.

2.2. Pollutants measurement

2.2.1. Ethical considerations

The exact sites where the campaign took place were not revealed and shall remain unnamed to avoid possible negative impacts of the findings reported here. The only information provided is the general location where the study was performed. The efforts are aligned with the ethical guidelines for wastewater-based surveillance set forth by the Sewage Analysis Core Group Europe to help minimize risk to communities and citizens [30].

2.2.2. Monitoring campaign

The study was conducted to monitor the presence of Human Use Antibiotics (HUS) in 2 geographic points of a river, in the northeast region of Portugal. The first (upstream) and second (downstream) points were located, respectively, 400 m before and 400 m after the discharge of the wastewater treated in the WWTP. Figure S1 illustrates the region and locations. On-site inspection was performed to ensure that only WWTP discharge existed between the selected points.

Polar Organic Chemical Integrative Samplers (POCIS), purchased from Environmental Sampling Technology (St. Joseph, MO USA), were used to monitor the presence of pharmaceuticals in river water near the WWTP. These samplers are loaded with three POCIS containing 200 mg of Oasis HLB (Water Corporation, Milford, MA USA) sorbent, mounted within a stainless-steel deployment canister. The device was deployed upstream and downstream the WWTP effluent, remaining there for 3 weeks. Once the deployment canister was recovered from the sampling site, each device was removed and wrapped in aluminum foil for protection and stored on ice until further analysis. It was then thoroughly cleaned with distilled water to remove any organic matter, grease, or embedded arthropods and subsequently stored at −20 °C until analysis. After retrieval, new POCIS were installed upon collection to continue the monitoring. The procedure was performed 3 times, amounting to around 2.25 months of analysis and 18 samples (3 samples per location each month). The experimental setup allowed for triplicate results in each location, ensuring the reliability of the measurements. The exact period of deployment in 2023 was between May 31st to June 21st (first period), June 21st to July 12th (second period), and July 12th to August 2nd (third period).

2.2.3. Analysis of drugs and metabolites

The POCIS were processed, and the concentration of the analytes was determined based on the Group 1 EPA (U.S. Environmental Protection Agency) 1694 method for determination of pharmaceutics and personal care products concentration [31]. Samples were processed at the Nebraska Water Sciences Laboratory, drugs and their metabolites underwent extraction from each hydrophilic-lipophilic balance (HLB) sorbent following established protocols [32], resulting in triplicate results for each location. Before extraction, each POCIS device underwent disassembly, and the HLB sorbent was carefully transferred to gravity-flow chromatography columns. Approximately 10 mL of acetonitrile rinsed any residual sorbent from the membrane into the chromatography column. Target compounds were then eluted from the sorbent using 70 mL of acetonitrile, gradually passing through the resin into glass evaporation tubes (RapidVap N_2, Labconco, St. Joseph, Missouri USA). Each extract and lab reagent blank (LRB) was spiked with 100 μL of 0.1 ng/μL surrogate spike, and 100 μL of 0.1/1 ng/μL analyte spike was added to the lab-fortified blank (LFB). The solvent was evaporated from all samples using the rapid evaporation apparatus (RapidVap Vacuum Dry Evaporation System, Labconco, St. Joseph, Missouri USA) until approximately 1 mL of solvent remained. The sampler extract was quantitatively transferred to glass test tubes using additional acetonitrile (*ca.* 2 mL), the resultant mixture was blown down under a stream of nitrogen gas to 500 μL. All samples were then spiked with 200 μL of internal standard (250 μL of carbamazepine-$^{13}C_6$, MDMA-d5, and MDA-d5, sulfamethazine-$^{13}C_6$, caffeine-$^{13}C_3$, morphine-d3, methadone-d3, oxycodone-d6, hydrocodone-d6, and temazepam-d5). The spiked extract was further evaporated under nitrogen to a final volume of 100 μL and mixed with 400 μL of distilled deionized water for a final ratio of 20:80 acetonitrile/water. The samples were then centrifuged at 12,000 rpm for 10 min and transferred into an autosampler vial containing a 300 μL silanized glass insert. Drug compounds, labeled surrogates, and internal standards were procured from Sigma-Aldrich (St. Louis, Missouri, USA) or Cerilliant (Round Rock, Texas, USA). Detailed information on how the surrogate spike, analyte spike, and internal standard spike were prepared can be consulted in Text S1. Quantification of drugs and metabolites was performed on a Xevo TQS-Micro (Waters Corporation, Midford, MA, USA) triple quadrupole mass spectrometer with a Uni-spray™ ionization source. Gradient separation occurred using a Waters Acquity Premier BEH C18 VanGuard Fit reverse phase UPLC column (50 mm x 2.1 mm with 1.7 μm particle size) at a temperature of 40 °C and a flow rate of 0.6 mL/min. Mobile phases used to separate the compounds of interest were (A) 0.3 % (v/v) formic acid and 0.1 % (w/v) ammonium formate in water and (B) 50 % methanol/50 % acetonitrile for a total run of 12 min per sample. The non-isocratic run is illustrated in Figure S2. Uni-spray™ ionization operated under the conditions shown in Table S2; and mass transitions, fragmentor voltages, collision energies, and instrument detection limits for each compound are detailed in Table S2.

The data was processed in Python using the libraries pandas (v. 2.2.2), seaborn (v. 0.13.2), matplotlib (v. 3.9.0) for graphics, scipy (v. 1.13.1), and numpy (v. 1.26.4). The correlations between substances were defined based on the Spearman correlation rank, and Tukey's honestly significant difference (HSD) allowing to dive further into which pollutants were present in concerning amounts.

2.3. Synthesis of CNTs

The CNTs were prepared according to a previous work [29]. The nanomaterials were synthesized by chemical vapor deposition (CVD) using iron oxide supported on alumina as a metal catalyst, prepared by sol-gel method [1]. In brief, two separate solutions were prepared: one comprising 20 mL of ethanol containing 10 mmol of $FeCl_2{\cdot}4\ H_2O$, and the other consisting of 80 mL of ethylene glycol with 20 mmol of $FeCl_3{\cdot}6\ H_2O$. Each solution was individually stirred and heated, with the former at 80 °C and the latter at 60 °C, before being cooled to room temperature. Subsequently, both solutions were combined with 6.6 g of alumina and thoroughly mixed. The resulting mixture underwent heating at 60 °C for 2 h, followed by further heating until reaching 120 °C, resulting in a gel-like consistency, and finally heated to 210 °C until a dry powder was obtained. The synthesized powder underwent calcination, initially at 300 °C for 12 h, and then at 600 °C for 24 h in air atmosphere, yielding iron oxide supported on alumina, denoted as IO/Al_2O_3 catalyst.

The CVD process was carried out in a one-chamber reactor, as schematically shown in Figure S3. The reactor is equipped with three independent heating zones and 2 crucibles. The upper crucible was loaded with 5 g of model polyolefin (LDPE in this case) and the lower crucible was loaded with 1 g of metal catalyst. The synthesis was performed for 1 h at 850 °C in the lower zone where CVD occurs, with a N_2 flow of 50 mL min^{-1}. The reactor was purged with N_2 for 2 h before the synthesis to ensure an inert atmosphere. The recovered material was named $CNT@IO/Al_2O_3$. The nanomaterial was further purified to remove the metal catalyst remaining from the synthesis. The procedure was carried out in a well-stirred three-necked round bottom flask equipped with a reflux condenser loaded with 1 g of CNTs and 50 mL of H_2SO_4 (50 *v/v*%) solution. The mixture remained stirring for 3 h at 140 °C, and the solid recovered was washed with distilled water until the rinsing waters reached the natural pH. The solid recovered from purification was named $CNTW@IO/Al_2O_3$. The characterization of these materials was already published in a previous work [29].

2.4. Synthesis of composite membranes

The composite polymeric membranes with the CNTs were fabricated adapting the procedure described in a previous work [33]. In a solution comprising 0.070 g of polyvinylpyrrolidone (PVP) dissolved in 6.0 mL of 1-methyl-2-pyrrolidone (NMP), 0.234 g of the powder material ($CNT@IO/Al_2O_3$ or $CNTW@IO/Al_2O_3$) was incorporated. This mixture underwent sonication for 3 h at room temperature. Following this, 1.07 g of poly(vinylidene fluoride) (PVDF) was introduced, and polymerization took place in a stirred glass flask maintained at 40 °C for 48 h The resultant polymer solution was then left unstirred overnight at room temperature before being spread onto a glass plate using a casting knife

film applicator (Elcometer 3580, Warren) set to a thickness of 100 μm. Subsequently, the spread solution was immersed in distilled water for coagulation, resulting in a composite PVP/PVDF@CNT (from CNT@IO/Al_2O_3) and PVP/PVDF@CNTW (from CNTW@IO/Al_2O_3) membranes. These membranes were cut into pieces measuring 1.64 cm in inner diameter and possessing an effective area of 2.10 cm^2, defined by the reactor dimensions as shown in Figure S4. These pieces were stored in distilled water until further use to avoid drying and subsequent deterioration. The composite membrane PVP/PVDF@IO/Al_2O_3 (from IO/Al_2O_3) was prepared following a similar procedure using a different amount of material, 0.09 g in this case. The amount corresponded to the theoretical quantity of CVD catalyst present in the PVP/PVDF@CNT membrane. A membrane without additives (polymeric membrane only) was also prepared and named PVP/PVDF.

2.5. Characterization techniques

The characterization techniques used here were based on previous works focused on solid materials and composite membranes [34–37]. The textural properties of the composite membranes were determined from the analysis of N_2 adsorption-desorption isotherms recorded at 77 K in a Quantachrome NOVATOUCH LX4 adsorption analyzer. The apparent surface area was determined by applying the Brunaeur-Emmet-Teller (BET) equation in the appropriate data range (p/p^0 = 0–0.35). The total pore volume (V_T) was calculated from the volume adsorbed at a relative pressure of 0.98, which corresponds to the sum of meso- and micropore volumes according to Gurvitch's rule [38].

The membrane morphology was investigated by Scanning Electron Microscopy (SEM) using a High Resolution (Schottky) Environmental Scanning Electron Microscope with X-Ray Microanalysis and Electron Backscattered Diffraction analysis (FEI Quanta 400 FEG ESEM / EDAX Genesis X4M). Samples were coated with an Au/Pd thin film, by sputtering, using the SPI Module Sputter Coater equipment when applicable (samples with low conductivity). The coating process was performed for 80 s with a current of 15 mA in Argon atmosphere. The cross-section characterization of the membranes was performed using membranes cut under cryogenic conditions through immersion in liquid nitrogen. The images were processed using ImageJ software to determine the average membrane thickness (10 measurements). Thermogravimetric Analysis (TGA) was performed on a simultaneous TGA-DSC thermobalance (TGA/DSC STARe SYSTEM 1100, Mettler-Toledo, S.A.E.) using a flow rate of 100 mL min^{-1} of nitrogen or air and a heating rate of 10 °C min^{-1}. Differential thermogravimetric (DTG) results were obtained by calculating the first derivative of mass loss concerning temperature (wt. % $°C^{-1}$) and processed using OriginLab software. The elemental analysis (CHNS) was carried out in a Flash 2000 analyzer (Thermo Fisher Scientific, Massachusetts, USA), provided with a thermal conductivity detector (TCD).

The hydrophilicity/hydrophobicity characteristic was obtained by measurements of the water contact angle, by the sessile-drop methodology, using an Attention (model theta) optical tensiometer for image acquisition, adapting a methodology described elsewhere [39]. The recorded images were processed using ImageJ software. The average contact angle was estimated from 3 droplets placed in different sites on the membrane surface.

The overall membrane porosity was calculated by a gravimetric method, following a procedure reported by Smolders and Franken [40]. The dry weight of the membranes was recorded, and they were immersed in isopropyl alcohol (IPA) overnight, so the solvent could penetrate the membrane pores. After this process, the membrane weight was recorded and registered. The porosity was calculated according to Eq. (1),

$$\varepsilon = \frac{(m_w - m_d)/\rho_{IPA}}{\frac{m_d}{\rho_d} + \frac{m_w - m_d}{\rho_{IPA}}} \cdot 100 \quad (1)$$

in which m_w and m_d represents the weight of the membranes, wet and dry, respectively, and ρ_{IPA} and ρ_P are IPA (0.786 g cm^{-3}) and polymer (1.78 g cm^{-3}) densities. The experiment was carried out in triplicate for each composite membrane.

The bubble point method, adapted from the literature [36], was used to measure the largest pore size of the composite membranes. In brief, the membrane is saturated with IPA following the same procedure used to determine porosity. The membrane is then fixated in the reaction apparatus, and the pressure is slowly increased on one side using an inert gas (nitrogen). At a certain point, the liquid starts to leave the membrane pores, and gas bubbles can be observed on the opposite side of the membrane. The gas pressure required to start this phenomenon is known as bubble point. From this experiment, the largest pore diameter can be calculated according to Eq. (2),

$$d_{pore} = \frac{4 \cdot \gamma \cdot cos\theta}{P_{bubble}} \quad (2)$$

in which γ is the surface tension of the liquid (2.17 mN m^{-1} for IPA), θ is the contact angle between the liquid and the pore wall, and P_{bubble} (bar) represents the bubble pressure. The experiment was carried out with three individual membranes to determine the average pore diameter.

2.6. Intensified filtration experiments

2.6.1. Experimental setup

The experiment was carried out by adapting a system reported in other studies [33], and the setup used here is shown in Figure S5 (dead-end mode). For the experiments, the flask containing the model solution was loaded with SMX (10 μg mL^{-1}) and a stoichiometric amount of H_2O_2 (44.3 μg mL^{-1}), calculated based on Eq. (3). The model solution pH was adjusted to 3.5 by means of H_2SO_4 (0.5 M) addition to meet the optimized conditions for hydroxyl radical formation from H_2O_2 [41].

$$C_{10}H_{11}N_3O_3S + 33\ H_2O_2 \rightarrow 10\ CO_2 + 36\ H_2O + H_2SO_4 + 3\ HNO_3 \quad (3)$$

The flask loaded with model solution remained stirring throughout the experiment. The HPLC pump (model) with a flow set to 1 mL min^{-1} was responsible for pumping the liquid through a heated column set to 80 °C. For this purpose, the recirculation bath had the temperature adjusted to 82 °C to ensure the desired temperature upon entering the reactor. The composite membrane was placed inside the reactor shown in Figure S5, and the reaction start was considered upon seeing the first liquid droplet on the permeating side of the membrane. Samples were collected periodically, considering enough volume to perform the pertinent analytical analyses. Considering the 20 mL sample collected at each time of interest and the flow, collections started 10 min before the time of interest and proceeded 10 min later. For example, the sample collection for 60 min started at 50 min and continued until 70 min. Following this logic, the collections were performed at 0, 50–70 (60), 110–130 (120), 230–250 (240), 350–370 (360), and 470–490 (480) min. The permeate flux was monitored along the reaction, and calculated according to Eq. (4),

$$J_W = \frac{\Delta W}{A \cdot \Delta t} \quad (4)$$

In which J_W is the permeate flux (L m^{-2} h^{-1}), ΔW is the mass of solution that passes through the membrane, A is the effective area of the membrane (m^2), and Δt is the sampling time (min). Pure filtration experiments and H_2O_2 decomposition experiments were performed in the absence of H_2O_2 and pollutants, respectively. The pollutant mass removal rate was calculated based on Eq. (5),

$$m_{Removed} = J_W \cdot ([SMX]_i - [SMX]_o) \quad (5)$$

In which $[SMX]_i$ is the concentration of SMX in the reactor inlet, and $[SMX]_o$ is the concentration of SMX in the reactor outlet. All experiments were performed in triplicate, and the result reported the average

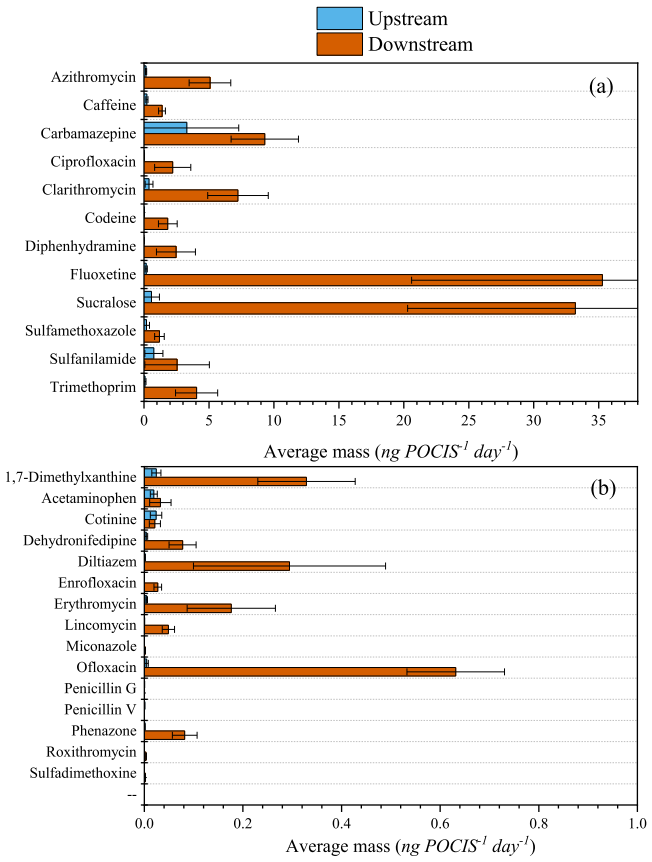

Fig. 1. Average amount ($n = 3$) of pollutants extracted from POCIS upstream and downstream during May-August 2023. Compounds found in higher concentration (a) and lower concentration (b).

obtained for each experimental point. The standard deviations were all below 5 %.

2.6.2. *Analytical techniques for treatment experiments*

The concentration of SMX was monitored during the reaction using a Jasco HPLC system at a wavelength of 254 nm (UV-2075 Plus detector). For this determination, a BiPhenyl column (BPH 5 μm 150 × 2.1 mm) and 0.3 mL min^{-1} flow (PU-2089 Plus) of an A: B mixture of acetonitrile (A) and ultrapure water acidified with 0.1 wt.% formic acid (B) were used. The readings were performed in a 9-minute isocratic run (10:90). The concentration of H_2O_2 was followed by adapting a methodology used in previous works [1]. In brief, a 0.5 mL reaction sample was added into a 5 mL volumetric flask previously loaded with 0.1 mL $TiOSO_4$ and 1 mL H_2SO_4 (0.5 M). The resultant mixture was analyzed at 405 nm using a spectrophotometer T70 from PG Instruments Ltd. (Lutterworth, United Kingdom). TOC analysis was carried out using a Shimadzu TOC-L CSN analyzer.

3. Results and discussion

3.1. *Monitoring campaign: average results*

Fig. 1 shows the average mass (nanograms per day) of pollutants accumulated at each location during the complete study (2.25 months), and Table S3 provides detailed results. Some compounds studied were not detected in any location (ampicillin, danofloxacin, digoxigerim, digoxin, flumequine, lomefloxacin, norfloxacin, norgestimate, ormetoprim, oxacillin, penicillin acid, sarafloxacin, sulfachloropyridazine, sulfadiazine, sulfamerazine, sulfamethiazole, and sulfathiazole). For all the pollutants measured, the average mass (and thus concentration) downstream of WWTP discharge increased significantly. In some cases (enrofloxacin, miconazole, roxithromycin, and sulfadimethoxine), the compounds were not present upstream and were introduced in the river water afterward, most likely due to the wastewater discharge of the WWTP. Overall, the results indicate that the WWTP is not adequately equipped to remove these pollutants from urban wastewater, as is the case of most WWTPs [42], which can negatively affect the water quality and compromise this resource for possible reuse with irrigation of food crops.

Moreover, most of the compounds that saw increased concentrations in the river water after the WWTP are used as antibiotics and antidepressants. The adverse effects of antibiotic presence in river waters have been widely studied in the literature, highlighting antibiotic resistance as one of the main issues that can be related to antibiotic presence in water bodies [43,44]. For instance, antibiotic resistance occurs when bacteria and other microorganisms evolve and are no longer sensitive to medicine. The outcome is the existence of infections that are harder to treat, increasing the risk of death [45]. The effects of antidepressants on the water ecosystem are not completely understood. However, recent literature reported the effects of fluoxetine (also detected in this work) on the photosensitivity and primary production of the suspended algae community. Aquatic invertebrates and vertebrates may also be affected by exposure to fluoxetine [46].

The results obtained for Tukey's HSD analysis using the mass of pollutants in the same location through the months is shown in Figure S6. The analysis highlighted the presence of carbamazepine at significant levels compared to other compounds upstream of the WWTP. Carbamazepine is a common antiepileptic drug that humans exclusively use, and its presence in river water may be used to indicate discharge of treated sewage [47]. The river studied here crosses a small city (30,000 inhabitants), and it isn't straightforward to analyze the source of carbamazepine in this location. One possible explanation could be related to the existence of illegal domestic wastewater disposal [48,49]. Downstream the WWTP, sucralose and fluoxetine were present in statistically significantly higher amounts than all other compounds. The presence of sucralose can be ascribed to its widespread usage as an artificial sweetener in food, drugs, and beverages. Several studies reported the presence of sucralose in surface waters and even in drinking water, which can be harmful to human health. Some studies reported that sucralose exposition, even at low concentrations, can exacerbate senescence and atherosclerosis [50]. The presence of fluoxetine in river water after WWTPs has also been reported in other works [51,52]. Fluoxetine is the most used antidepressant, and the human body metabolizes only a fraction of the compound. Some studies have analyzed the effects of fluoxetine in aquatic vertebrate and invertebrate species, including a deeper analysis of the effect of this drug on fish. Among the concerns related to fluoxetine presence in river water, the neurotoxicity and genetic and biochemical changes have been highlighted [53]. Despite the statistically significant carbamazepine level in WWTPs upstream, it's important to highlight that the carbamazepine amount increased downstream. In addition, despite sucralose and fluoxetine being detected at higher levels downstream, other compounds were also detected in moderate-high levels after the discharge point of the WWTP (azithromycin, carbamazepine, clarithromycin, sulfamethoxazole, and trimethoprim).

The Spearman correlation rank was used to explore further correlations of substance use in the community studied in this work, and the result is shown in Fig. 2 for both locations. The rank correlates individual compounds in a population and can change from −1 (inverse correlation) to 1 (direct correlation). The result obtained for location 1 revealed different correlation levels between the substances. Carbamazepine, ciprofloxacin, clarithromycin, dehydronifedipine, fluoxetine, phenazone, sucralose, sulfamethoxazole, sulfanilamide, thiabendazole and trimethoprim were identified with high correlation between themselves (> 0.46) and moderate correlation with other substances except for penicillin G and V, and cotinine, which correlated among them (>

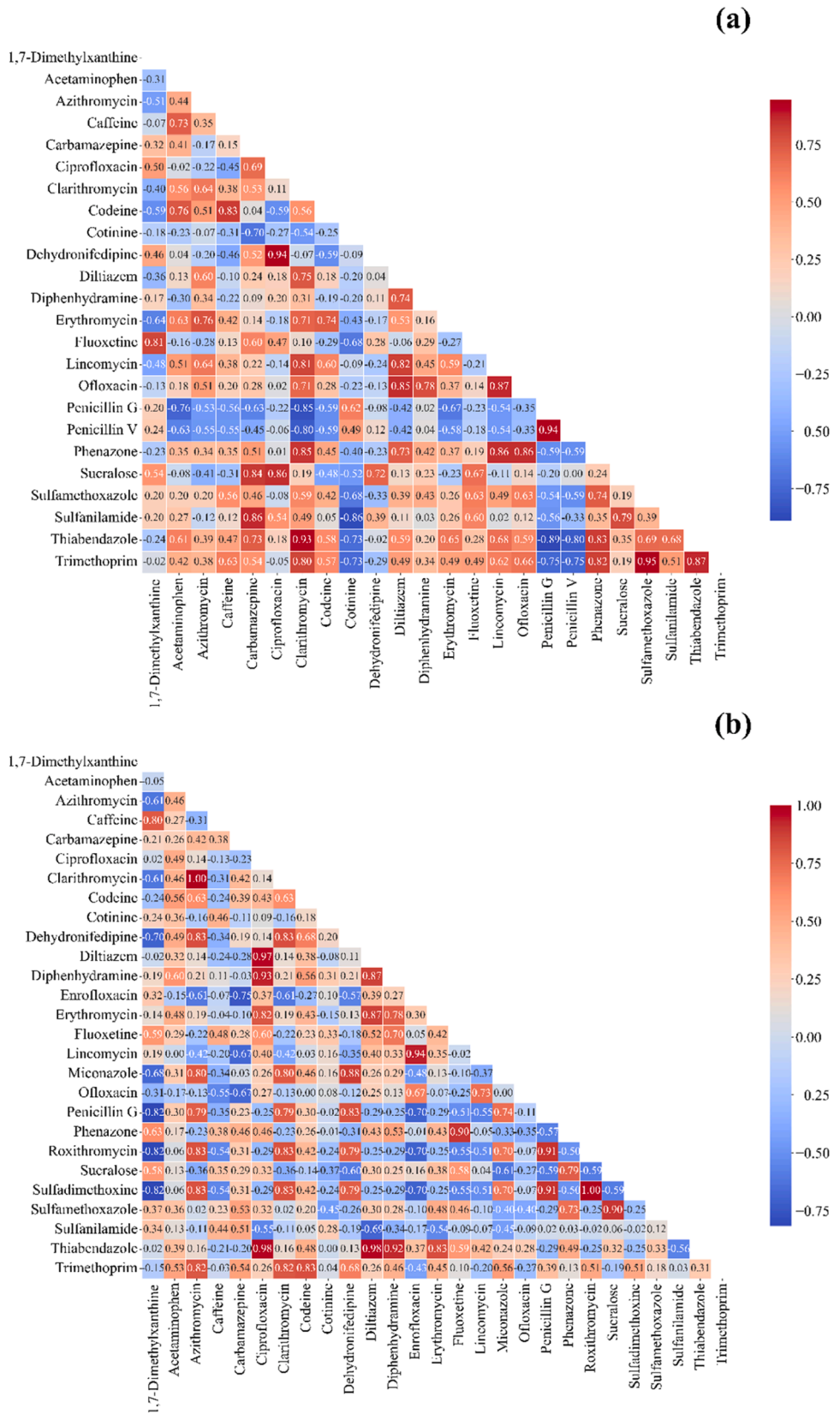

Fig. 2. Spearmans correlation rank obtained for pollutants found (a) upstream and (b) downstream ($n = 3$).

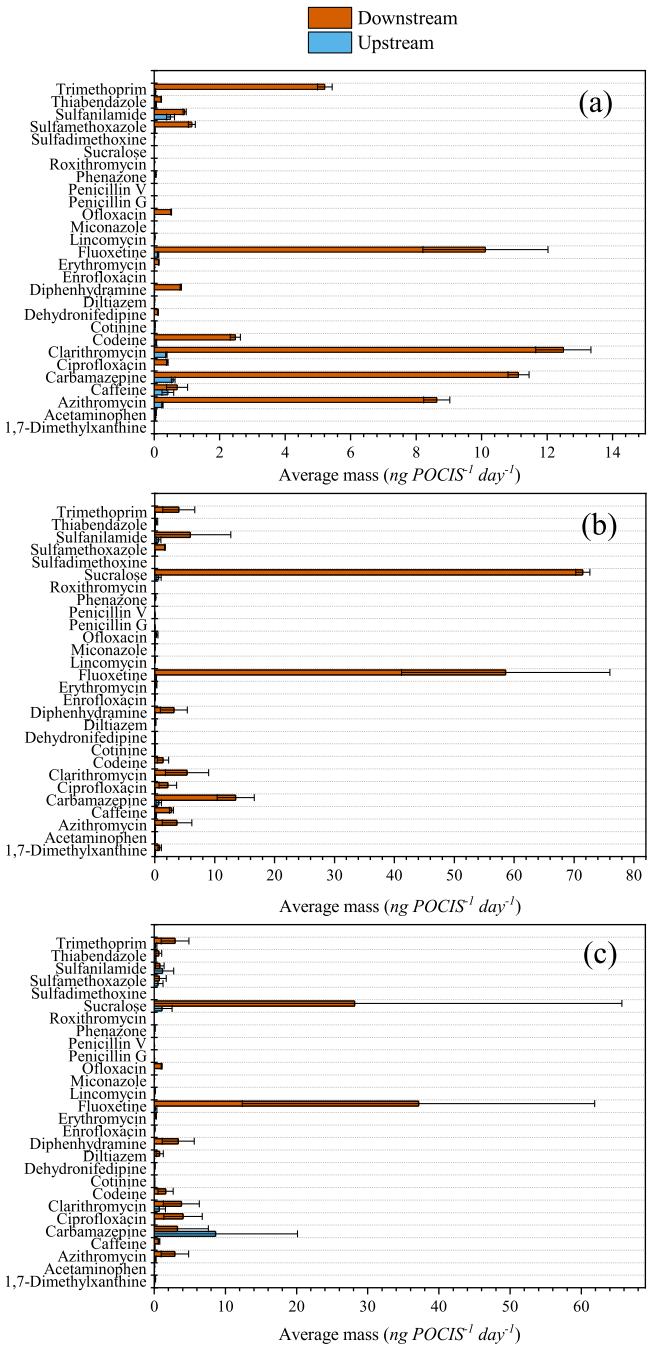

Fig. 3. Average amount ($n = 3$) of pollutant found upstream and downstream in the (a) first period, (b) second period, and (c) third period of study.

0.49). Location 2 presented more marked correlations than location 1, with less moderate correlations. Acetaminophen, azithromycin, carbamazepine, clarithromycin, ciprofloxacin, codeine, dehydrodifedipine, diphenhydramine, erythromycin, fluoxetine, roxithromycin, sucralose, thiabendazole, and trimethoprim correlated. For the second location, penicillin G presented more correlation with other substances such as azithromycin, clarithromycin, dehydronifedipine, miconazole, and a strong correlation with sulfadimethoxine and roxithromycin. Overall, the analysis revealed a strong correlation between antibiotics and antidepressants. The obtention of moderate correlations for location 1 and more variability in sample 2 can be explained by the introduction of chemical species in more quantities by the treated wastewater discharged into the river. In the second location, the correlation between substances was stronger, pointing out the compounds with higher disturbance in concentration on river waters due to the action of a third party, the wastewater discharge in this case. The variations of compound amounts during the campaign can be another reason for the variety of results obtained in the Spearman rank.

The high correlation between these substances, some of controlled use, suggests that the most likely source of contamination is the health care units located in the community. Other possible sources include improper antibiotic discharge, and the antibiotic fraction that is not digested by humans.

3.2. Monitoring campaign: the mass of substances in different periods

The results obtained for samples processed in each separated period presented significant differences in the concentration of the compounds studied, and the results are shown in Fig. 3. The compounds detected in both locations in the first 2 periods were in higher amounts downstream. However, the analysis of the last period samples showed that carbamazepine was present in more quantities upstream than downstream. It is important to highlight that the error associated with the measurement of carbamazepine in this sample was high, which could be the reason for such a result. The results obtained for the first period (May 20th - June 17th, 2023) revealed that the compounds clarithromycin, carbamazepine, azithromycin, and fluoxetine had highest increase downstream compared to upstream. The amount of chemical substances found in POCIS for the first period was in the range 9.54×10^{-3}–13.7 ng POCIS^{-1} day^{-1}.

The results from the second monitoring period showed a high concentration of fluoxetine and sucralose, reaching values above 1 μg downstream. The result obtained for these 2 compounds in this period overshadows the other results. In addition, the amount of antibiotics and other compounds also oscillated compared to the first period. For instance, carbamazepine was the compound with about the same amount as in the first period. The amount of chemical substances in the second period studied was in the range 1.36×10^{-2}–84.7 ng POCIS^{-1} day^{-1}. At last, the results obtained for the third period showed sucralose and fluoxetine again surpassing 1 μg downstream, and the rest of the compounds followed a similar trend to the second period. The amount of chemical substances ranged from 1×10^{-2} – 84.5 ng POCIS^{-1} day^{-1}. The varying amounts of compounds during the campaign, especially concerning the downstream location, are connected to several factors, some of which are not possible to determine. However, the amount of compounds found in each period increased throughout the study, which is certainly a result of the number of people residing in the community increasing during the summer.

3.3. Characterization of materials

3.3.1. Summary of CNTs characterization

The CNTs and the CVD catalyst (IO/Al2O3) used as filling materials were characterized and reported in a previous publication, as well as the catalytic activity of those materials in CWPO of paracetamol (PCM) [29]. The IO/Al_2O_3 catalyst is a composite material composed of 78 % alumina, 19 % hematite (α-Fe_2O_3), and 3 % magnetite (Fe_3O_4), as identified through semi-quantitative XRD analysis. CNTW@IO/Al_2O_3 synthesized from polyolefins using the IO/Al_2O_3 catalyst exhibits multi-walled structures with bamboo-like morphology, as shown in Figure S7. The CNTs have hollow cavities, with outer diameters measured at 37 ± 12 nm for CNTW@IO/Al_2O_3, and with wall thickness of 28 ± 3 nm. Purification with H_2SO_4 effectively removes metal and alumina impurities, increasing the carbon content from 58.3 wt.% (CNT@IO/Al_2O_3) to 92.5 wt.% (CNTW@IO/Al_2O_3). Cementite content decreases after purification, from 32 % in CNT@IO/Al_2O_3 to 19 % in CNTW@IO/Al_2O_3 according to semi-quantitative XRD analysis (Figure S8), consistent with removing metallic impurities during acid washing. The transition from iron oxides to cementite during CNT growth occurs due to hydrogen reduction conditions during CCVD.

Table 1
Textural properties, contact angle and pore size of the synthesized membranes.

Membrane	S_{BET} ($m^2\ g^{-1}$)	V_T ($mm^3\ g^{-1}$)	Porosity, ε (%)	Contact angle (°)	d_{pore} (μm)
PVP/PVDF*	22	0.0289	84	55	11
PVP/PVDF@IO/Al_2O_3¥	34	0.0494	84	73	10
PVP/PVDF@CNT£	34	0.0516	70	88	4
PVP/PVDF@CNTW	29	0.0537	74	87	5

* PVP = polyvinylpyrrolidone; PVDF = poly(vinylidene fluoride).
¥ IO = iron oxide.
£ CNT = carbon nanotube.

Despite the reduction in the inorganic content in CNTW@IO/Al_2O_3, the material still presents a magnetic response to the presence of a strong magnet, which is related to the cementite phase formed during the CVD process and encapsulated within the CNT walls.

Textural properties, including BET surface area and total pore volume, remain relatively unaffected by the purification process. For instance, the BET surface area of CNTW@IO/Al_2O_3 is 66 $m^2\ g^{-1}$, compared to 67 $m^2\ g^{-1}$ for CNT@IO/Al_2O_3. These values suggest that the removal of impurities does not significantly alter the porosity or surface characteristics of the CNTs.

3.3.2. Textural properties and morphology of polymeric composite membranes

Figure S9 shows the N_2 adsorption-desorption isotherms obtained for the membranes. The results demonstrated that the membranes did not significantly develop micro and mesoporosity, which is the typical range of porosities analyzed by this technique. Table 1 shows the results obtained for surface area and total pore volume, along with overall porosity, bubble point, and contact angle. Interestingly, the surface area increased when filling materials were incorporated into the polymeric membrane. The surface area modification upon the addition of CNTs and CVD catalyst is closely related to the dispersions and interactions between the solid materials and the casting solution due to the influence on non-solvent/solvent exchange during the formation of the porous structure. In this case, the porosity change and surface area increase will be closely related to the textural properties of the materials used for the filling. Other works have also reported increasing surface area upon the addition of CNTs in polymeric membrane structures [36,54].

The overall porosity was analyzed by a gravimetric method, and the result is displayed in Table 1. The results indicate that adding filling material to the membrane composition decreased the porosity, which is related to the agglomeration of the material in bundles or to the formation of microvoids. The smallest porosity decrease observed for the membrane prepared with CVD catalyst can be explained by the smallest amount of solid material used to prepare this membrane. Notably, the amount of CVD catalyst was added to mimic the amount of metals present in CNTs membrane, which was calculated based on previous characterization reported elsewhere [29]. Interestingly, the membrane porosity of PVP/PVDF@CNTW was higher than that of PVP/PVDF@CNT, which is related to the surface chemistry modification experienced by the CNTs during the purification procedure. Other studies have also reported a decrease in overall porosity due to the addition of filling material in composite membranes. The largest pore size (d_{pore}) of the membranes obtained by the bubble point method revealed the influence of the filling materials used in each membrane and the surface chemistry. For instance, the addition of filling materials

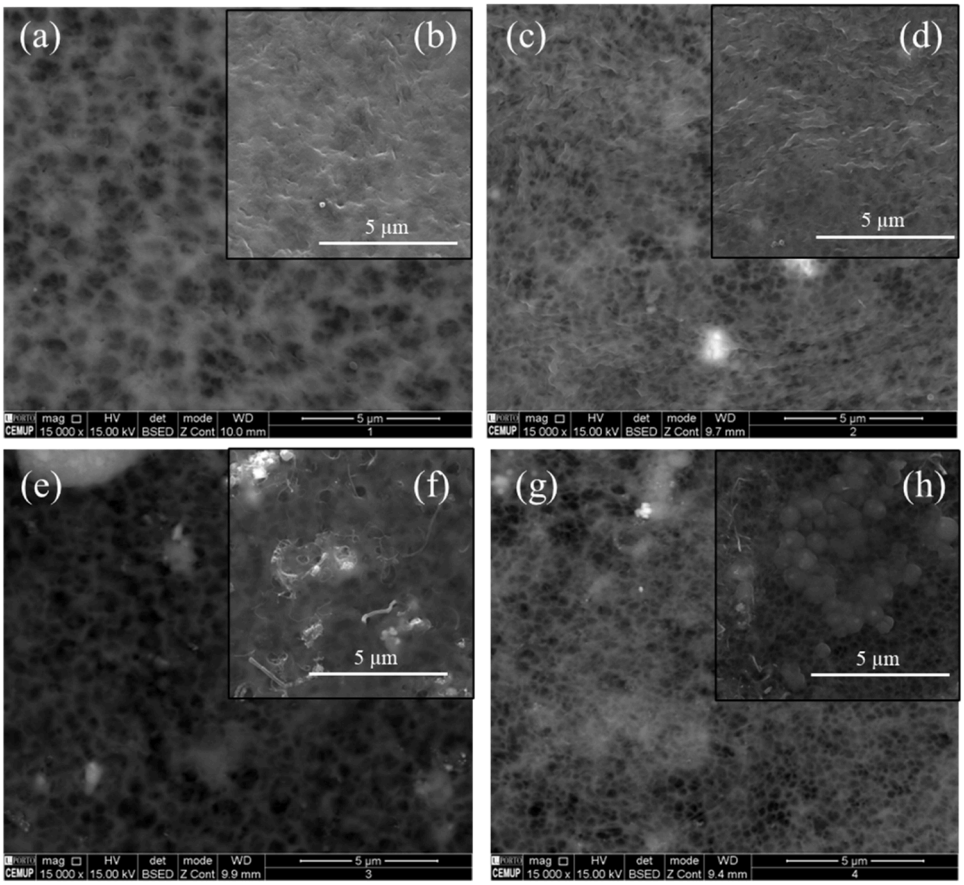

Fig. 4. SEM images of (a,b) PVP/PVDF, (c,d) PVP/PVDF@IO/Al_2O_3, (e,f) PVP/PVDF@CNT, and (g,h) PVP/PVDF@CNTW. Figures (a,c,e,g) are from the BSE mode and figures (b,d,f,h) from the SE mode. (PVP = polyvinylpyrrolidone; PVDF = poly(vinylidene fluoride); IO = iron oxide; CNT = carbon nanotube).

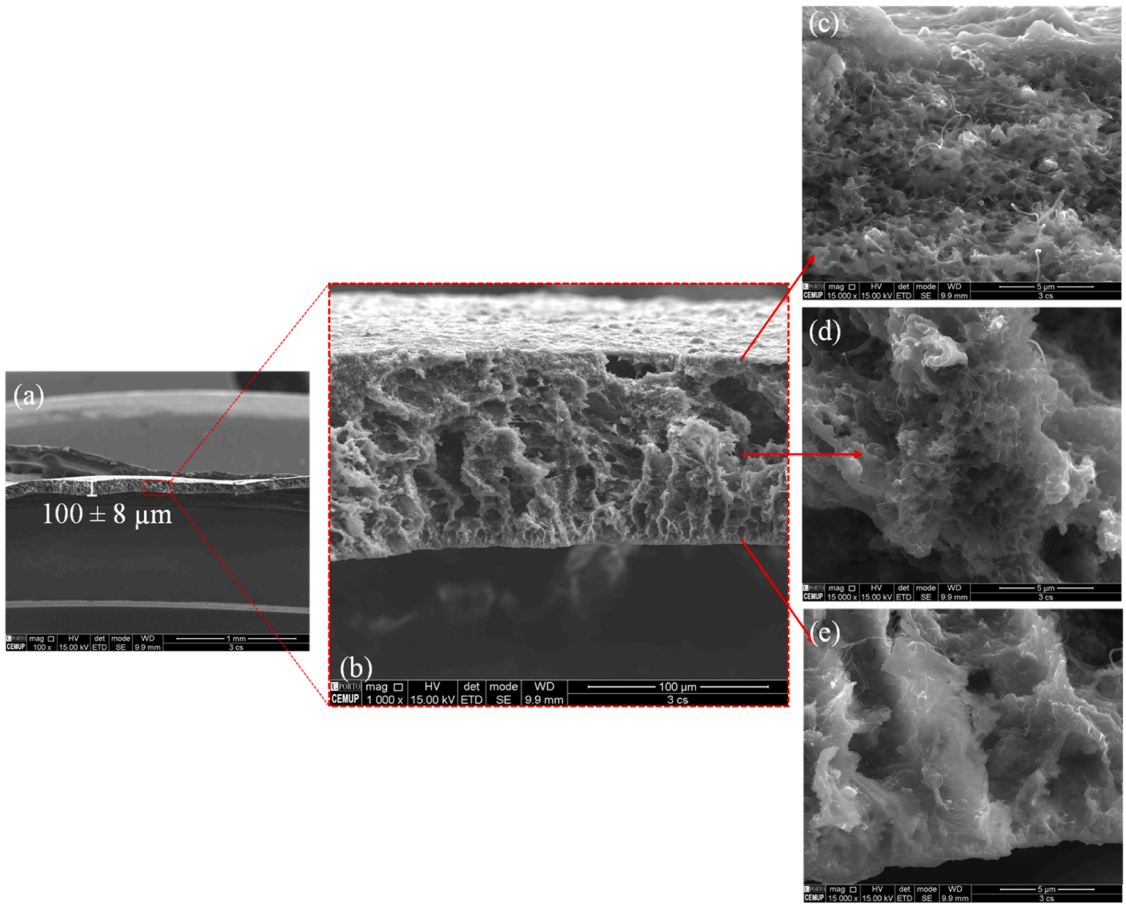

Fig. 5. SEM image of the cross-section of PVP/PVDF@CNT (cut under cryogenic conditions). (a) whole membrane cross-section, (b) zoom in the pore network, (c) upper, (d) middle, and (e) lower regions of the zoomed membrane showing CNTs distribution. (PVP = polyvinylpyrrolidone; PVDF = poly(vinylidene fluoride); CNT = carbon nanotube).

decreased the largest pore size value for all membranes, with a more pronounced decrease for membranes loaded with CNTs. The smallest pore size (*ca.* 4.5 µm) was obtained for the membrane prepared with the purified CNTs (CNTW). The decrease in the largest pore size upon loading the membrane with CNTs was also reported in other studies [36] .

The membrane surface wettability was investigated by measuring the static water contact angle. The images were acquired using the built-in software of the equipment and analyzed using ImageJ, and the results are shown in Table 1. The result showed that blank membrane is hydrophilic (55°), which is related to the presence of PVP in the membrane formulation [36]. Several works have already studied the incorporation of PVP in PVDF membranes to increase hydrophilicity and improve water compatibility [3,55,56]. In this work, composite membranes increased the contact angle when filled with CVD catalyst (73°), pristine CNTs (88°), and purified CNTs (87°) compared to the PVP/PVDF membrane (55°). The increase in water contact angle correlates to the hydrophilic/hydrophobic nature of the materials used to fabricate the composite membranes. Furthermore, literature suggests that increased roughness due to the incorporation of a solid powder in composite membranes can affect the water contact angle [55]. The highest increase in water contact angle observed for PVP/PVDF@CNT compared to PVP/PVDF@IO/Al_2O_3 is related to the hydrophobic nature of CNTs and the mild hydrophilic nature of the CVD catalyst. Despite the increase in contact angles observed upon modification, the composite membranes still have a higher hydrophilic character, which is of utmost importance considering the use of the membranes in the application here studied for wastewater treatment purposes.

The SEM images recorded for all membranes are shown in Fig. 4. The result obtained for the surface analysis of PVP/PVDF (Fig. 4b) and PVP/PVDF@IO/Al_2O_3 (Fig. 4d) composite membranes revealed smooth surfaces in both membranes. The backscattered electron imaging (BSE) performed in both samples revealed a porous network inside the membranes, as shown in Figs. 4a and 4c. The images do not allow to determine precisely the average membrane pore size but corroborate with previous results showing that PVP/PVDF@IO/Al_2O_3 have smaller pores (d_{pore} obtained for PVP/PVDF@IO/Al_2O_3 is 1 µm smaller than d_{pore} for the PVP/PVDF membrane). The EDS result recorded for the samples revealed the presence of carbon and fluor in the PVP/PVDF membrane, and the presence of metals (Al, Fe) and oxygen in PVP/PVDF@IO/Al_2O_3 due to the use of iron oxide catalyst for its preparation (Figure S10). Au and Pd signals observed in EDS comes from the coating performed to increase the sample conductivity, so the images could be acquired in SEM.

Fig. 4 clearly shows the presence of CNTs on the surface of both membranes. PVP/PVDF@CNT (Figure S11a) showed the CNTs more dispersed in the sample compared to PVP/PVDF@CNTW (Figure S11b), which can be related to the highest compatibility of the CNTs with no purification compared to the purified one. The poor dispersibility of CNTs in the polymeric membrane can be confirmed in Fig. 4c, in which a cluster of CNTs can be seen in the left central side of the image. The BSE results of the CNTs composite membranes revealed a pore size smaller than in PVDF/PVP@IO/Al_2O_3 and PVP/PVDF membranes, which was also confirmed with d_{pore} measurements (Table 1). The BSE result obtained for the membranes also showed how efficient the acid washing procedure is to remove metals from CNTs since the amount of metal in

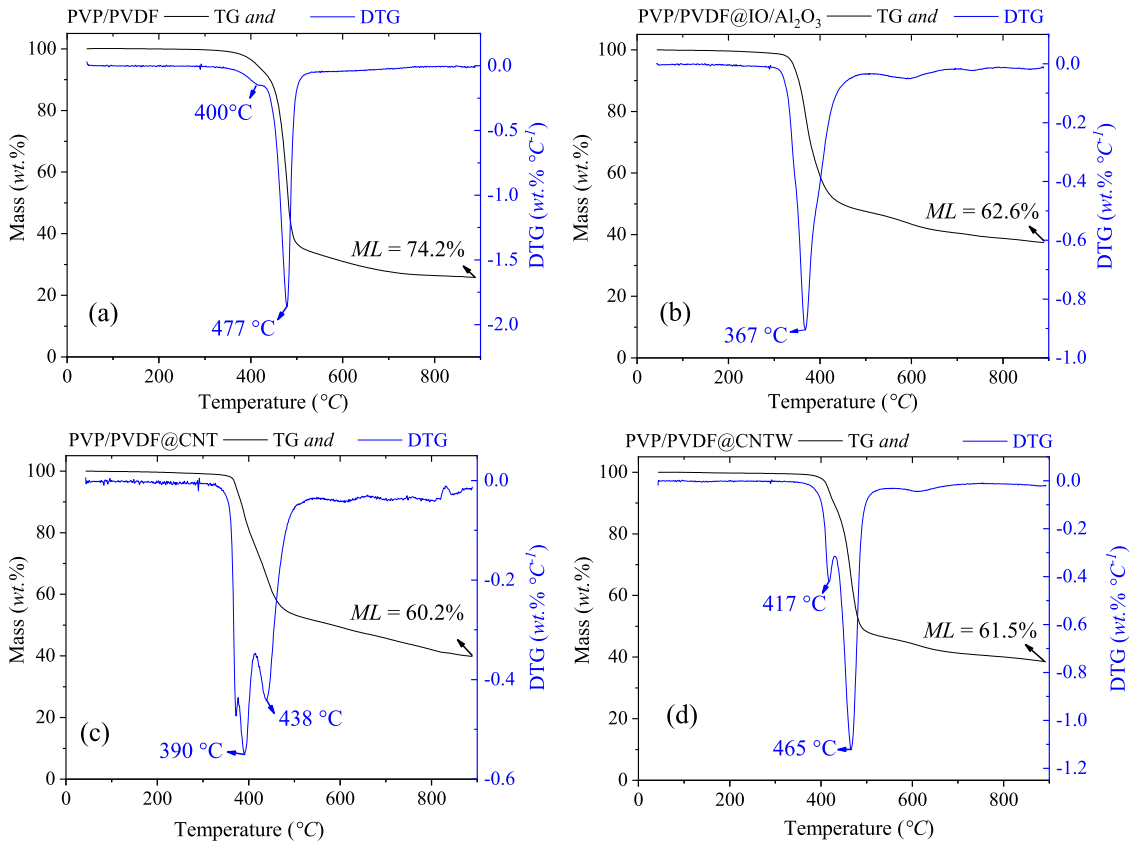

Fig. 6. TGA results in N_2 atmosphere for (a) PVP/PVDF, (b) PVP/PVDF@IO/Al_2O_3, (c) PVP/PVDF@CNT, and (d) PVP/PVDF@CNTW. (PVP = polyvinylpyrrolidone; PVDF = poly(vinylidene fluoride); IO = iron oxide; CNT = carbon nanotube).

the membrane clearly changed, comparing Figures S12a and c (SE mode) with Figures S12 b and d (BSE mode). The results obtained for the cross-section of PVP/PVDF@CNT, which showed more compatibility between additive and polymeric matrix, are shown in Fig. 5. The result demonstrates that membrane thickness is about 100 ± 8 μm, which is close to the desired considering the synthesis procedure. Fig. 5b confirmed the results observed previously with BSE, in which the pore structure inside the membrane and the smooth surface can be observed. The uniform CNTs distribution inside the polymeric structure can be confirmed with images from the top (Fig. 5c), middle (Fig. 5d), and lower (Fig. 5e) regions of the membrane cross-section.

3.3.3. *Thermal properties and elemental composition of polymeric composite membranes*

The results obtained in TGA and DTG are shown in Fig. 6(N_2) and Figure S13 (air). The results demonstrate that all membranes have a thermal stability up to *ca.* 300 °C. The main mass loss peaks observed for the different samples were correlated with the filling material, with significant differences. For the blank membrane (Fig. 6a) the mass loss peak was at *ca.* 477 °C, which agrees with literature [57]; and represents the PVDF decomposition. Another peak is observed in the PVP/PVDF membrane around 390 °C, ascribed to the thermal decomposition of PVP [36]. The addition of metal catalyst in the polymeric membrane (PVP/PVDF@IO@Al_2O_3) caused the early degradation of the PVDF polymer since the mass loss peak was shifted to the left (*ca.* 370 °C; Fig. 6b). The phenomenon is related to the metal-polymer interaction that catalyzes thermal degradation under certain conditions [58,59]. The metal particles from CNT@IO/Al_2O_3, given that it is not purified, present in PVP/PVDF@CNT also affected the thermal decomposition of this membrane, shifting the two mass loss peaks to *ca.* 390 °C and 438 °C, ascribed to PVP and PVDF polymer degradation (Fig. 6c), respectively. Lastly, the membrane prepared with the purified CNTs (PVP/PVDF@CNTW; Fig. 6d) demonstrated a thermal behavior closer to the original membrane with the main mass loss peak for PVDF being observed at *ca.* 465 °C. The final mass losses observed in an inert atmosphere agree with literature, resulting in *ca.* 60 wt.% for membranes prepared with additives [33].

The results obtained for TGA in air (Figure S13) revealed a mass loss peak (*ca.* 650 °C) ascribed to the degradation of the CNTs incorporated in the polymeric matrix (Figure S11c and Figure S11d) [29]. The elemental composition (C, H, N, S, and O) obtained for the membranes is shown in Table S4. The results revealed increased carbon content in composite membranes prepared with purified CNTs compared to the pristine membrane (49 % C content in PVP/PVDF@CNTW vs. 42 % C content in PVP/PVDF). The other elements studied here did not present significant changes, including oxygen. The remaining *ca.* 25–27 % obtained in all membranes can be mainly ascribed to fluoride content [60].

3.4. *Catalytic wet peroxide oxidation (CWPO) enhanced filtration*

3.4.1. *Pure filtration experiments and H_2O_2 decomposition ability*

The results obtained for pure filtration experiments with all membranes are shown in Fig. 7a. In general, the samples have poor filtration capacity. The PVP/PVDF@CNT membrane allowed the highest removal of SMX by pure filtration (or adsorption) at 1 h on stream. Nevertheless, the CNTs-enriched membrane rapidly saturated, and the removal of SMX dropped to *ca.* 20 % from 2 to 6 h on stream, decreasing to *ca.* 0 % by the 8-hour on stream mark. The remaining membranes did not result in significant filtration/adsorption capacity, with removals of SMX lower than 10 % during the entire experiment.

The capacity of the membranes to decompose H_2O_2 under continuous flow mode (in the absence of the pollutant) was evaluated and the results are displayed in Fig. 7b. As can be seen, the blank membrane (PVP/PVDF) did not display any significant activity toward the

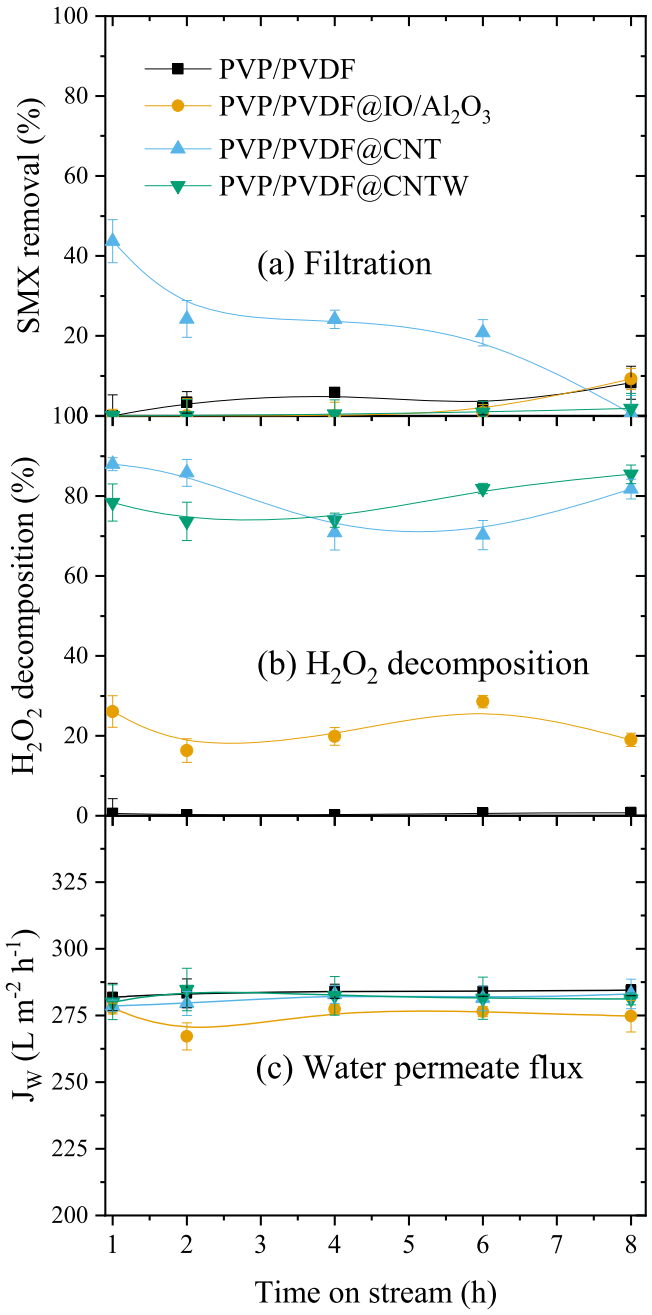

Fig. 7. (a) Pure filtration of sulfamethoxazole (SMX), (b) pure H_2O_2 decomposition (*i.e.* without SMX) and (c) water permeate flux in pure filtration experiments considering the different membranes upon time on stream. Conditions: Q = 1 mL min^{-1}, T = 80 °C, pH_0 = 3.5, [SMX] = 20 mg L^{-1}, $[H_2O_2]_0$ = 44.3 mg L^{-1}. Adsorption and H_2O_2 decomposition were carried out in the absence of H_2O_2 and SMX, respectively. (PVP = polyvinylpyrrolidone; PVDF = poly(vinylidene fluoride); IO = iron oxide; CNT = carbon nanotube).

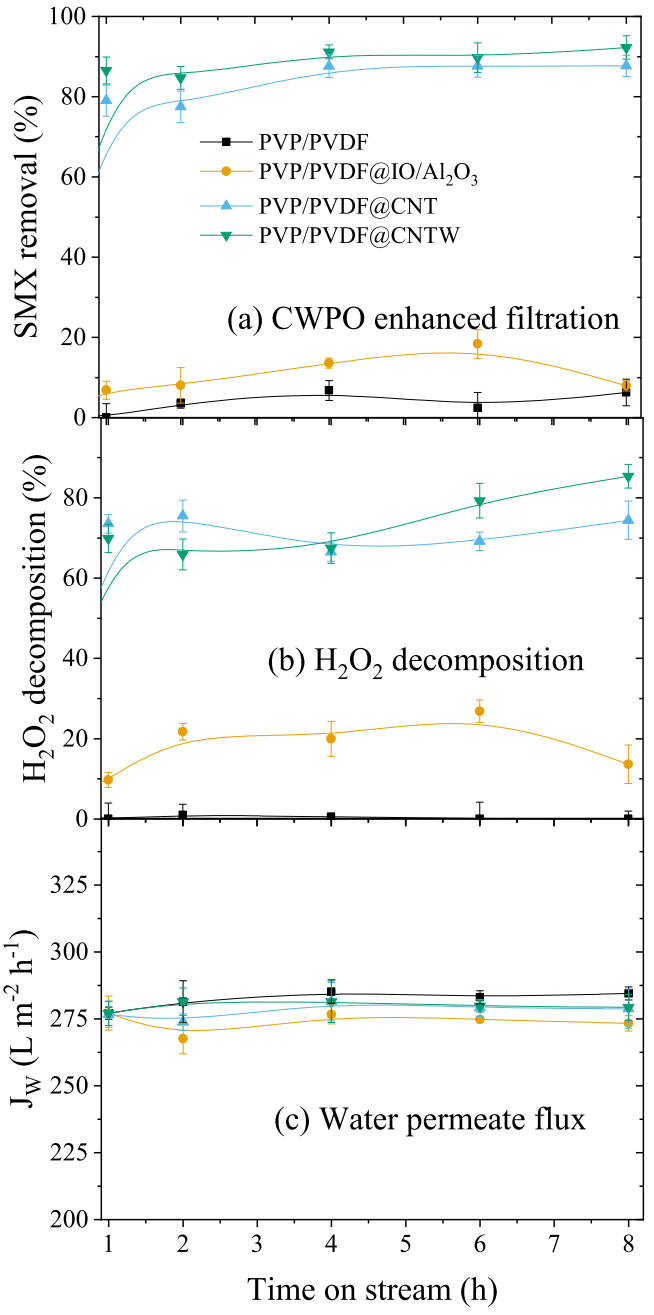

Fig. 8. CWPO-enhanced filtration runs. Removal of (a) SMX by CWPO enhanced filtration, (b) H_2O_2 decomposition, and (c) water permeate flux considering the different membranes upon time on stream. Conditions: Q = 1 mL min^{-1}, [SMX] =10 mg L^{-1}, $[H_2O_2]_0$ = 44.3 mg L^{-1}, T = 80 °C, pH_0 = 3.5. (PVP = polyvinylpyrrolidone; PVDF = poly(vinylidene fluoride); IO = iron oxide; CNT = carbon nanotube).

decomposition of H_2O_2 (< 1 %). The incorporation of the CVD catalyst (IO/Al_2O_3) allowed an increased decomposition of H_2O_2, maintaining consumption in the range of *ca.* 20–30 % during the entire experiment. The incorporation of both types of CNTs resulted in a much more relevant H_2O_2 consumption, with the composite membranes showing *ca.* 80–90 % of H_2O_2 consumption in the 8 h runs. The water permeate flux (J_W) was stable during the whole operation (Fig. 7c). No evident difference between as-synthesized and purified CNTs was verified. Given the differences between the CVD-catalyst composite membrane and the CNTs-enriched membrane, it is concluded that CNTs are the main active fraction of the composite membranes. Previous works have shown that carbon phases are active in the catalytic decomposition of H_2O_2 [1,61].

3.4.2. *CWPO enhanced filtration*

The CWPO-enhanced filtration results are shown in Fig. 8. The blank membrane (PVP/PVDF) barely resulted in a low SMX removal, with results below 10 % (Fig. 8a). The SMX removals by the blank membrane are equivalent to those observed during pure filtration runs (Fig. 7a). The blank membrane did not result in any H_2O_2 consumption (Fig. 8b), similar to what was previously observed for this membrane (Fig. 7b) in pure H_2O_2 decomposition experiments. Incorporating the CVD catalyst

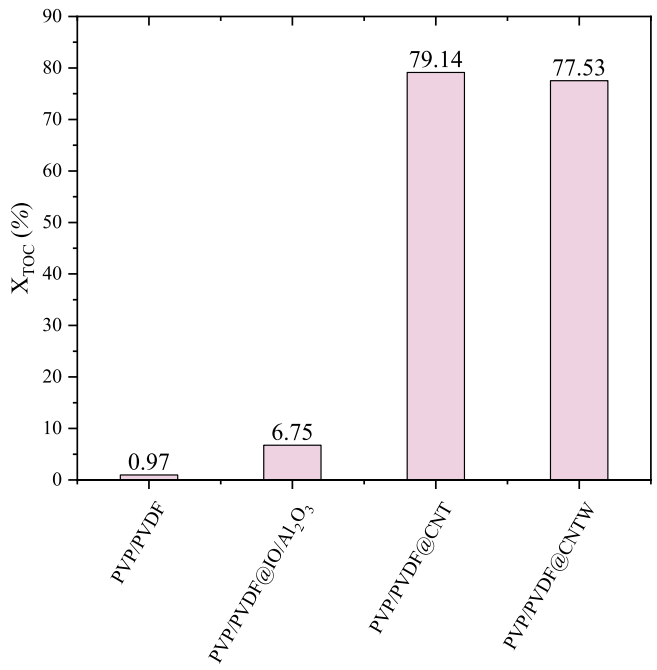

Fig. 9. TOC conversion obtained at 8 h of time on stream. (PVP = polyvinylpyrrolidone; PVDF = poly(vinylidene fluoride); IO = iron oxide; CNT = carbon nanotube).

slightly improved the SMX removal, resulting in 10–20 % removal during the 8 h of operation. Near the end of the operation (from 6 to 8 h), the SMX dropped from 20 % to 10 %, corresponding to the drop in H_2O_2 consumption observed for this membrane (Fig. 8b). Both membranes (PVP/PVDF and PVP/PVDF@IO/Al_2O_3) act poorly in SMX removal, either via pure or enhanced filtration system.

The incorporation of the CNTs, on the other hand, resulted in a significant increase in SMX removal. From 4 h onwards, the composite membranes maintained an SMX removal of *ca.* 85 % and 90 % (PVP/PVDF@CNT and PVP/PVDF@CNTW, respectively), which is equivalent to a pollutant mass removal of 2451 and 2551 mg m^{-2} h^{-1}, respectively. The decomposition of H_2O_2 was also much superior in the presence of the CNTs-enriched membranes, with H_2O_2 consumption maintained above 65 % during the whole operation (Fig. 8b). The water permeate flux (J_W) was stable during the whole operation (Fig. 8c). TOC was measured at 8 h of time on stream, when the system was already in steady state, and the results are shown in Fig. 9. The TOC abatement for both polymeric membranes loaded with CNTs reached >75 %, confirming the efficient degradation of the model pollutant. The pH measured at 8 h on stream reinforces the degradation of the model pollutant, dropping from an initial value of 3.5 in the reactor inlet to 3.1 in the reactor outlet. During pure filtration and H_2O_2 decomposition experiments, the pH remained unchanged after 8 h on the stream.

Similar results have been previously reported for composite polymeric membranes in AOPs-enhanced filtration. Ribeiro et al. (2022) reported the removal of 71 % of venlafaxine (1.97 mg m^{-2} h^{-1}) with activated persulfate oxidation and CNT-enriched membranes, achieving steady-state after 5 h of reaction [33]. Vieira et al. (2020) obtained 85–90 % removal of three micropollutants (ciprofloxacin, enrofloxacin, and ofloxacin, equivalent to 2.56–2.72 mg m^{-2} h^{-1}) using graphene oxide composite membranes for the activated persulfate oxidation, achieving steady state after 2 h of operation [39]. Nieto-Sandoval et al. (2023) reported steady-state removals (after 3 h) of 89, 92 and 72 % for metoprolol, venlafaxine and diclofenac, respectively, using carbon nitride composite membranes in photocatalysis [62], whereas a blank membrane allowed removals below 5 %. Ma et al. (2020) reported 65 % removal of SMX after 100 min of operation for the peroxymonosulfate oxidation using CNTs-enriched membranes [22]. Iron was measured in the final sample, and no metal was detected, showing that all membranes are stable for liquid-phase reactions in these conditions.

4. Conclusions

The results obtained from the monitoring campaign suggests that the studied WWTP contributes pharmaceuticals to receiving streams, and 27 out of 28 detected compounds were measured in higher amounts after the WWTP treated wastewater discharge into the river water. Among these micropollutants, antidepressants and antibiotics were detected in higher amounts, which could threaten the aquatic life and human health. Considering the complexity of the municipal wastewater arriving at the WWTP, one possible solution would be to install more advanced technologies to refine the wastewater treatment, so that most complex pollutants would be mineralized before discharge.

The results obtained for the CWPO intensified filtration solution herein investigated, using polymeric composite membranes loaded with carbonaceous materials showed significant efficiency towards the degradation of SMX in continuous flow mode. The characterization revealed that the filling carbonaceous material distribution in the composite membrane contributed to the highest efficiency observed on the membrane prepared with CNTs (washed and not washed). The similar performance between PVP/PVDF@CNT and PVP/PVDF@CNTW and lack of iron leaching in the reactor outlet enables to conclude that the PVP/PVDF@CNT membrane is the best one, since no acid washing step is needed to obtain the respective CNTs. In addition, the SEM images revealed that CNTs were uniformly distributed in the membrane, which was not verified for the PVP/PVDF@CNTW membrane.

The results presented in this work for the degradation of SMX in continuous flow mode by CWPO showed one efficient technology that can be used to reinforce facilities of WWTPs to improve the quality of the discharging effluents. Future works can assess other aspects related with the implementation on a large scale, such as evaluating the efficiency of the solution with milder temperatures and pH closer to the natural one.

CRediT authorship contribution statement

Adriano S. Silva: Writing – original draft, Visualization, Methodology, Investigation, Formal analysis, Conceptualization. **Paulo Zadra Filho:** Investigation, Formal analysis. **Ana Paula Ferreira:** Writing – review & editing, Investigation. **Fernanda F. Roman:** Writing – original draft. **Arthur P. Baldo:** Investigation, Formal analysis. **Madeleine Rauhauser:** Methodology, Investigation, Formal analysis. **Jose L. Diaz de Tuesta:** Writing – review & editing, Supervision. **Ana I. Pereira:** Writing – review & editing, Supervision. **Adrián M.T. Silva:** Writing – review & editing, Supervision. **Juliana M.T. Pietrobelli:** Supervision. **Marzhan S. Kalmakhanova:** Writing – review & editing. **Daniel D. Snow:** Writing – review & editing, Supervision, Project administration, Funding acquisition. **Helder T. Gomes:** Writing – review & editing, Supervision, Project administration, Funding acquisition.

Declaration of competing interest

The authors declare that they have no known competing financial interests or personal relationships that could have appeared to influence the work reported in this paper.

Acknowledgments

This work was financially supported by national funds through FCT/MCTES (PIDDAC): CeDRI, UIDB/05757/2020 (DOI: 10.54499/UIDB/05757/2020) and UIDP/05757/2020 (DOI: 10.54499/UIDB/05757/2020); CIMO, UIDB/00690/2020 (DOI: 10.54499/UIDB/00690/2020) and UIDP/00690/2020 (DOI: 10.54499/UIDP/00690/2020); SusTEC, LA/P/0007/2020 (DOI: 10.54499/LA/P/0007/2020). This work was

also supported by national funds through FCT/MCTES (PIDDAC): LSRE-LCM, UIDB/50020/2020 (DOI: 10.54499/UIDB/50020/2020) and UIDP/50020/2020 (DOI: 10.54499/UIDP/50020/2020); ALiCE, LA/P/0045/2020 (DOI: 10.54499/LA/P/0045/2020). Fernanda F. Roman acknowledges the national funding by FCT and the European Social Fund, FSE, through the individual research grant SFRH/BD/143224/2019. Adriano S. Silva was supported by the doctoral Grant SFRH/BD/151346/2021 and Ana Paula Ferreira by PRT/BD/153090/2021, financed by FCT with funds from NORTE2020, under MIT Portugal Program. Jose L. Diaz De Tuesta acknowledges the financial support through the program of Atracción al Talento of Comunidad de Madrid (Spain) for the individual research grant 2022-T1/AMB-23946. The authors are also grateful for the finantial support provided by Sociedade Ponto Verde for the project "Estudo técnico-económico para a valorização de resíduos de embalagens plásticas na produção de nanotubos de carbono" and by Fundação La Caixa for the project INOVÁGUA.

Supplementary materials

Supplementary material associated with this article can be found, in the online version, at doi:10.1016/j.ceja.2025.100707.

Data availability

Data will be made available on request.

References

[1] A.S. Silva, F.F. Roman, A.V. Dias, J.L. Diaz de Tuesta, A. Narcizo, A.P.F. da Silva, I. Çaha, F.L. Deepak, M. Bañobre-López, A.M.C. Ferrari, H.T. Gomes, Hybrid multi-core shell magnetic nanoparticles for wet peroxide oxidation of paracetamol: application in synthetic and real matrices, J. Environ. Chem. Eng. 11 (2023) 110806, https://doi.org/10.1016/j.jece.2023.110806.

[2] A. Yar, Ş. Parlayici, Carbon nanotubes/polyacrylonitrile composite nanofiber mats for highly efficient dye adsorption, Colloids. Surf. a Physicochem. Eng. Asp. 651 (2022), https://doi.org/10.1016/j.colsurfa.2022.129703.

[3] M.O. Mavukkandy, Q. Zaib, H.A. Arafat, CNT/PVP blend PVDF membranes for the removal of organic pollutants from simulated treated wastewater effluent, J. Environ. Chem. Eng. 6 (2018) 6733–6740, https://doi.org/10.1016/j.jece.2018.10.029.

[4] J. Ravi, M.H.D. Othman, T. Matsuura, M. Ro'il Bilad, T.H. El-badawy, F. Aziz, A. F. Ismail, M.A. Rahman, J. Jaafar, Polymeric membranes for desalination using membrane distillation: a review, Desalination 490 (2020), https://doi.org/10.1016/j.desal.2020.114530.

[5] S. Korkmaz, I.A. Kariper, Fog harvesting against water shortage, Environ. Chem. Lett. 18 (2020) 361–375, https://doi.org/10.1007/s10311-019-00950-5.

[6] Z. Noorimotlagh, A.S. Silva, J.L. Diaz de Tuesta, S.A. Mirzaee, S.S. Martínez, H. T. Gomes, Chapter 7 - Wastewater purification using advanced functionalized nanoparticles, in: S. ul Islam, C.M. Hussain, S.K. Shukla (Eds.), Antiviral and Antimicrobial Coatings Based on Functionalized Nanomaterials, Elsevier, 2023, pp. 223–283, https://doi.org/10.1016/B978-0-323-91783-4.00002-4.

[7] S.R. Penmetsa, B.K. Allam, D. Pise, P.K. Gautam, S. Banerjee, V. Kumar, Design and development of a pilot plant for the treatment of pharmaceutical wastewater containing molasses, Water. Pract. Technol. 19 (2024) 489–501, https://doi.org/10.2166/wpt.2024.004.

[8] G. Bertanza, R. Boiocchi, R. Pedrazzani, Improving the quality of wastewater treatment plant monitoring by adopting proper sampling strategies and data processing criteria, Sci. Total Environ. 806 (2022), https://doi.org/10.1016/j.scitotenv.2021.150724.

[9] R. Guibal, S. Lissalde, G. Guibaud, Experimental estimation of 44 pharmaceutical polar organic chemical integrative sampler sampling rates in an artificial river under various flow conditions, Environ. Toxicol. Chem. 39 (2020) 1186–1195, https://doi.org/10.1002/etc.4717.

[10] K. Godlewska, P. Stepnowski, M. Paszkiewicz, Pollutant analysis using passive samplers: principles, sorbents, calibration and applications. A review, Environ. Chem. Lett. 19 (2021) 465–520, https://doi.org/10.1007/s10311-020-01079-6.

[11] B. Mathon, M. Ferreol, A. Togola, S. Lardy-Fontan, A. Dabrin, I.J. Allan, P.F. Staub, N. Mazzella, C. Miège, Polar organic chemical integrative samplers as an effective tool for chemical monitoring of surface waters – results from one-year monitoring in France, Sci. Total Environ. 824 (2022), https://doi.org/10.1016/j.scitotenv.2022.153549.

[12] S. and D.A. and B.-H.S.L. and S.D.D. and M.L.M, A. Severson Marie, Onanong, Analysis of wastewater samples to explore community substance use in the United States: pilot correlative and machine learning study, JMIR Form. Res. 7 (2023) e45353, https://doi.org/10.2196/45353.

[13] L.D. Brunelle, A.L. Batt, A. Chao, S.T. Glassmeyer, N. Quinete, D.A. Alvarez, D. W. Kolpin, E.T. Furlong, M.A. Mills, D.S. Aga, De facto water reuse: investigating the fate and transport of chemicals of emerging concern from wastewater discharge through drinking water treatment using non-targeted analysis and suspect screening, Environ. Sci. Technol. 58 (2024) 2468–2478, https://doi.org/10.1021/acs.est.3c07514.

[14] C. Metcalfe, M.E. Hoque, T. Sultana, C. Murray, P. Helm, S. Kleywegt, Monitoring for contaminants of emerging concern in drinking water using POCIS passive samplers, Environ. Sci.: Process. Impacts 16 (2014) 473–481, https://doi.org/10.1039/c3em00508a.

[15] J. Xiong, Z. Wang, X. Ma, H. Li, J. You, Occurrence and risk of neonicotinoid insecticides in surface water in a rapidly developing region: application of polar organic chemical integrative samplers, Sci. Total Environ. 648 (2019) 1305–1312, https://doi.org/10.1016/j.scitotenv.2018.08.256.

[16] C. Metcalfe, M.E. Hoque, T. Sultana, C. Murray, P. Helm, S. Kleywegt, Monitoring for contaminants of emerging concern in drinking water using POCIS passive samplers, Environ. Sci.: Process. Impacts 16 (2014) 473–481, https://doi.org/10.1039/c3em00508a.

[17] E. Magi, M. Di Carro, C. Mirasole, B. Benedetti, Combining passive sampling and tandem mass spectrometry for the determination of pharmaceuticals and other emerging pollutants in drinking water, Microchem. J. 136 (2018) 56–60, https://doi.org/10.1016/j.microc.2016.10.029.

[18] S. Kim, A. Sin, H. Nam, Y. Park, H. Lee, C. Han, Advanced oxidation processes for microplastics degradation: a recent trend, Chem. Eng. J. Adv. 9 (2022), https://doi.org/10.1016/j.ceja.2021.100213.

[19] A.M. Chávez, A. Torres-Pinto, P.M. Álvarez, J.L. Faria, C.G. Silva, A.M.T. Silva, One-pot synthesis and immobilization of urea-derived graphitic carbon nitride onto ceramic foams for visible-light photocatalytic wet peroxide oxidation in water treatment, Chem. Eng. J. 481 (2024), https://doi.org/10.1016/j.cej.2023.148141.

[20] A. Torres-Pinto, A.M. Díez, C.G. Silva, J.L. Faria, M.Á. Sanromán, A.M.T. Silva, M. Pazos, Photoelectrocatalytic degradation of pharmaceuticals promoted by a metal-free gC3N4 catalyst, Chem. Eng. J. 476 (2023), https://doi.org/10.1016/j.cej.2023.146761.

[21] A.Santos Silva, F.F. Roman, R.S. Ribeiro, J. Garcia, H.T. Gomes, Beyond batch experiments: unveiling the potential of bimetallic carbon xerogels for catalytic wet peroxide oxidation of hospital wastewater in continuous mode, Environ. Sci. Pollut. Res. (2024), https://doi.org/10.1007/s11356-024-35546-2.

[22] H. Ma, G. Wang, Z. Miao, X. Dong, X. Zhang, Integration of membrane filtration and peroxymonosulfate activation on CNT@nitrogen doped carbon/Al2O3 membrane for enhanced water treatment: insight into the synergistic mechanism, Sep. Purif. Technol. 252 (2020), https://doi.org/10.1016/j.seppur.2020.117479.

[23] M. Hayyan, M.A. Hashim, I.M. Alnashef, Superoxide ion: generation and chemical implications, Chem. Rev. 116 (2016) 3029–3085, https://doi.org/10.1021/acs.chemrev.5b00407.

[24] Y. Li, X. Zheng, Q. Guo, X. Wang, L. Zhang, W. Zhu, Y. Luo, Activation of peroxymonosulfate by the CoFe/ZSM-5 for efficient sulfamethoxazole degradation, J. Environ. Chem. Eng. 10 (2022), https://doi.org/10.1016/j.jece.2021.107012.

[25] S. Ma, X. Zuo, J. Xiong, C. Ma, Z. Chen, Sulfamethoxazole removal enhancement from water in high-silica ZSM-5/ozonation synchronous system with low ozone consumption, J. Water. Process. Eng. 33 (2020), https://doi.org/10.1016/j.jwpe.2019.101083.

[26] J. Dang, W. Pei, F. Hu, Z. Yu, S. Zhao, J. Hu, J. Liu, D. Zhang, Z. Jing, X. Lei, Photocatalytic degradation and toxicity analysis of sulfamethoxazole using TiO2/BC, Toxics 11 (2023), https://doi.org/10.3390/toxics11100818.

[27] R.S. Ribeiro, Z. Frontistis, D. Mantzavinos, D. Venieri, M. Antonopoulou, I. Konstantinou, A.M.T. Silva, J.L. Faria, H.T. Gomes, Magnetic carbon xerogels for the catalytic wet peroxide oxidation of sulfamethoxazole in environmentally relevant water matrices, Appl. Catal. B 199 (2016) 170–186, https://doi.org/10.1016/j.apcatb.2016.06.021.

[28] Y. Deng, R. Zhao, Advanced Oxidation Processes (AOPs) in wastewater treatment, Curr. Pollut. Rep. 1 (2015) 167–176, https://doi.org/10.1007/s40726-015-0015-z.

[29] J.L. Diaz de Tuesta, A.S. Silva, F.F. Roman, L.F. Sanches, F.A. da Silva, A.I. Pereira, A.M.T. Silva, J.L. Faria, H.T. Gomes, Polyolefin-derived carbon nanotubes as magnetic catalysts for wet peroxide oxidation of paracetamol in aqueous solutions, Catal. Today 419 (2023) 114162, https://doi.org/10.1016/j.cattod.2023.114162.

[30] J. Prichard, W. Hall, E. Zuccato, P. De Voogt, N. Voulvoulis, K. Kummerer, B. Kasprzyk-Hordern, A. Barbato, A. Parabiaghi, F. Hernandez, J. van Wel, K.V. Thomas, K. Fent, M. Mardal, S. Castiglioni, Ethical research guidelines for wastewater-based epidemiology and related fields, 2015. https://www.euda.europa.eu/drugs-library/ethical-research-guidelines-wastewater-based-epidemiology-and-related-fields_en (accessed November 27, 2024).

[31] I. Ferrer, J.A. Zweigenbaum, E.M. Thurman, Analysis of 70 Environmental Protection Agency priority pharmaceuticals in water by EPA Method 1694, J. Chromatogr. A 1217 (2010) 5674–5686, https://doi.org/10.1016/j.chroma.2010.07.002.

[32] D.A. Alvarez, J.D. Petty, J.N. Huckins, T.L. Jones-Lepp, D.T. Getting, J.P. Goddard, S.E. Manahan, Development of a passive, *in situ*, integrative sampler for hydrophilic organic contaminants in aquatic environments, Environ. Toxicol. Chem. 23 (2004) 1640–1648, https://doi.org/10.1897/03-603.

[33] R.S. Ribeiro, O. Vieira, R. Fernandes, F.F. Roman, J.L. Diaz de Tuesta, A.M.T. T. Silva, H.T. Gomes, Synthesis of low-density polyethylene derived carbon nanotubes for activation of persulfate and degradation of water organic micropollutants in continuous mode, J. Environ. Manage 308 (2022) 114622, https://doi.org/10.1016/j.jenvman.2022.114622.

[34] S. Moretto, A.Santos Silva, J.L. Diaz de Tuesta, F.F. Roman, R. Cortesi, A.R. Bertão, M. Bañobre-López, M. Pedrosa, A.M.T. Silva, H.T. Gomes, Comprehensive characterization and development of multi-core shell superparamagnetic nanoparticles for controlled delivery of drugs and their kinetic release modelling,

Mater. Today Chem. 33 (2023) 101748, https://doi.org/10.1016/j.mtchem.2023.101748.
[35] A.S. Silva, J.L. Diaz de Tuesta, T. Sayuri Berberich, S. Delezuk Inglez, A.R. Bertão, I. Çaha, F.L. Deepak, M. Bañobre-López, H.T. Gomes, Doxorubicin delivery performance of superparamagnetic carbon multi-core shell nanoparticles: pH dependence, stability and kinetic insight, Nanoscale 14 (2022) 7220–7232, https://doi.org/10.1039/D1NR08550F.
[36] T.L.S. Silva, S. Morales-Torres, J.L. Figueiredo, A.M.T. Silva, Multi-walled carbon nanotube/PVDF blended membranes with sponge- and finger-like pores for direct contact membrane distillation, Desalination 357 (2015) 233–245, https://doi.org/10.1016/j.desal.2014.11.025.
[37] F.F. Roman, J.L. Diaz de Tuesta, F.K.K. Sanches, A.S. Silva, P. Marin, B.F. Machado, P. Serp, M. Pedrosa, A.M.T. Silva, J.L. Faria, H.T. Gomes, Selective denitrification of simulated oily wastewater by oxidation using Janus-structured carbon nanotubes, Catal. Today 420 (2023) 114001, https://doi.org/10.1016/j.cattod.2023.01.008.
[38] Adsorption by Powders and Porous Solids, Elsevier, 1999, https://doi.org/10.1016/B978-0-12-598920-6.X5000-3.
[39] O. Vieira, R.S. Ribeiro, M. Pedrosa, A.R. Lado Ribeiro, A.M.T. Silva, Nitrogen-doped reduced graphene oxide – PVDF nanocomposite membrane for persulfate activation and degradation of water organic micropollutants, Chem. Eng. J. 402 (2020) 126117, https://doi.org/10.1016/j.cej.2020.126117.
[40] K. Smolders, A.C.M. Franken, Terminology for membrane distillation, Desalination 72 (1989) 249–262, https://doi.org/10.1016/0011-9164(89)80010-4.
[41] A. Fischbacher, C. von Sonntag, T.C. Schmidt, Hydroxyl radical yields in the Fenton process under various pH, ligand concentrations and hydrogen peroxide/Fe(II) ratios, Chemosphere 182 (2017) 738–744, https://doi.org/10.1016/j.chemosphere.2017.05.039.
[42] J. Matesun, L. Petrik, E. Musvoto, W. Ayinde, D. Ikumi, Limitations of wastewater treatment plants in removing trace anthropogenic biomarkers and future directions: a review, Ecotoxicol. Environ. Saf. 281 (2024), https://doi.org/10.1016/j.ecoenv.2024.116610.
[43] S. Reddy, K. Kaur, P. Barathe, V. Shriram, M. Govarthanan, V. Kumar, Antimicrobial resistance in urban river ecosystems, Microbiol. Res. 263 (2022), https://doi.org/10.1016/j.micres.2022.127135.
[44] P. Grenni, Antimicrobial resistance in rivers: a review of the genes detected and new challenges, Environ. Toxicol. Chem. 41 (2022) 687–714, https://doi.org/10.1002/etc.5289.
[45] S. Moles, S. Gozzo, M.P. Ormad, R. Mosteo, J. Gómez, F. Laborda, J. Szpunar, Long-term study of antibiotic presence in Ebro River Basin (Spain): identification of the emission sources, Water 14 (2022), https://doi.org/10.3390/w14071033.
[46] R.A. Mole, B.W. Brooks, Global scanning of selective serotonin reuptake inhibitors: occurrence, wastewater treatment and hazards in aquatic systems, Environ. Pollut. 250 (2019) 1019–1031, https://doi.org/10.1016/j.envpol.2019.04.118.
[47] S.K. Haack, J.W. Duris, L.R. Fogarty, D.W. Kolpin, M.J. Focazio, E.T. Furlong, M. T. Meyer, Comparing wastewater chemicals, indicator bacteria concentrations, and bacterial pathogen genes as fecal pollution indicators, J. Environ. Qual. 38 (2009) 248–258, https://doi.org/10.2134/jeq2008.0173.
[48] R.L. Seiler, S.D. Zaugg, J.M. Thomas, D.L. Howcroft, Caffeine and pharmaceuticals as indicators of waste water contamination in wells, Ground Water 37 (1999) 405–410, https://doi.org/10.1111/j.1745-6584.1999.tb01118.x.
[49] T.A. Ternes, Occurrence of drugs in German sewage treatment plants and rivers, Water Res. 32 (1998) 3245–3260, https://doi.org/10.1016/S0043-1354(98)00099-2.
[50] C. Wang, Q. Zheng, X. Yang, Occurrence and removal of acesulfame and sucralose in the drinking water treatment plants along the Yangtze River, Water Sci. Technol. Water Supply 19 (2019) 1305–1312, https://doi.org/10.2166/ws.2018.191.
[51] M.J. Fernandes, P. Paíga, A. Silva, C.P. Llaguno, M. Carvalho, F.M. Vázquez, C. Delerue-Matos, Antibiotics and antidepressants occurrence in surface waters and sediments collected in the north of Portugal, Chemosphere 239 (2020), https://doi.org/10.1016/j.chemosphere.2019.124729.
[52] F. Zindler, S. Tisler, A.K. Loerracher, C. Zwiener, T. Braunbeck, Norfluoxetine is the only metabolite of fluoxetine in zebrafish (Danio rerio) embryos that accumulates at environmentally relevant exposure scenarios, Environ. Sci. Technol. 54 (2020) 4200–4209, https://doi.org/10.1021/acs.est.9b07618.
[53] D. Correia, I. Domingues, M. Faria, M. Oliveira, Effects of fluoxetine on fish: what do we know and where should we focus our efforts in the future? Sci. Total Environ. 857 (2023) https://doi.org/10.1016/j.scitotenv.2022.159486.
[54] C. Ji, J. Hou, V. Chen, Cross-linked carbon nanotubes-based biocatalytic membranes for micro-pollutants degradation: performance, stability, and regeneration, J. Memb. Sci. 520 (2016) 869–880, https://doi.org/10.1016/j.memsci.2016.08.056.
[55] I. Purnawan, D. Angputra, S.C. Debora, E.F. Karamah, A. Febriasari, S. Kartohardjono, Polyvinylidene fluoride membrane with a polyvinylpyrrolidone additive for tofu industrial wastewater treatment in combination with the coagulation–flocculation process, Membranes 11 (2021), https://doi.org/10.3390/membranes11120948.
[56] Z. Guo, X. Xu, Y. Xiang, S. Lu, S.P. Jiang, New anhydrous proton exchange membranes for high-temperature fuel cells based on PVDF-PVP blended polymers, J. Mater. Chem. A Mater. 3 (2015) 148–155, https://doi.org/10.1039/c4ta04952g.
[57] A.J. de Jesus Silva, M.M. Contreras, C.R. Nascimento, M.F. da Costa, Kinetics of thermal degradation and lifetime study of poly(vinylidene fluoride) (PVDF) subjected to bioethanol fuel accelerated aging, Heliyon 6 (2020), https://doi.org/10.1016/j.heliyon.2020.e04573.
[58] M. Bustamante-Torres, D. Romero-Fierro, B. Arcentales-Vera, S. Pardo, E. Bucio, Interaction between filler and polymeric matrix in nanocomposites: magnetic approach and applications, Polymers 13 (2021), https://doi.org/10.3390/polym13172998.
[59] S. Lee, S.-J. Shin, H. Baek, Y. Choi, K. Hyun, M. Seo, K. Kim, D.-Y. Koh, H. Kim, M. Choi, Dynamic metal-polymer interaction for the design of chemoselective and long-lived hydrogenation catalysts, 2020. https://www.science.org.
[60] R. Gayatri, A.N.S. Fizal, E. Yuliwati, M.Z. Zailani, J. Jaafar, M.S. Hossain, M. Zulkifli, W. Taweepreda, A.N. Ahmad Yahaya, Effect of polyvinylidene fluoride concentration in PVDF-TiO2-PVP composite membranes properties and its performance in bovine serum albumin rejection, Case Stud. Chem. Environ. Eng. 9 (2024), https://doi.org/10.1016/j.cscee.2024.100620.
[61] A.S. Silva, J.L. Diaz de Tuesta, A. Henrique, F.F. Roman, D. Omralinov, H. Steldinger, J. Gläsel, B.J.M. Etzold, J.A.C. Silva, A.M.T. Silva, A.I. Pereira, H. T. Gomes, 3D printed photopolymer derived carbon catalysts for enhanced wet peroxide oxidation, Chem. Eng. J. (2024) 156574, https://doi.org/10.1016/j.cej.2024.156574.
[62] J. Nieto-Sandoval, A. Torres-Pinto, M. Pedrosa, M. Munoz, Z.M. de Pedro, C. G. Silva, J.L. Faria, J.A. Casas, A.M.T. Silva, Application of g-C3N4-PVDF membrane for the photocatalytic degradation of micropollutants in continuous flow mode: impact of water matrix, J. Environ. Chem. Eng. 11 (2023), https://doi.org/10.1016/j.jece.2023.110586.